Ultrasonics 99 (2019) 105952

Contents lists available at ScienceDirect

Ultrasonics

journal homepage: www.elsevier.com/locate/ultras

Measurement of velocity and attenuation of ultrasonic guided wave for real-time estimation of cure-dependent anisotropic viscoelastic properties of carbon fiber-reinforced plastics

Koichi Mizukami*, Takahiro Ikeda, Keiji Ogi

Department of Civil and Environmental Engineering, Ehime University, 7908577 Bunkyo-cho 3, Matsuyama-shi, Ehime, Japan

ARTICLE INFO

Keywords:
Guided wave
Composite material
Cure monitoring
Viscoelastic material
Anisotropic material

ABSTRACT

An ultrasonic guided wave-based cure monitoring technique is developed to estimate cure-dependent anisotropic viscoelastic properties of carbon fiber reinforced plastics (CFRPs). The guided wave propagating in the transverse direction of a CFRP was measured during a cure process and the energy velocity and attenuation were obtained by signal processing. A micromechanics model and transfer matrix method were used to express the energy velocity and attenuation as functions of only the complex Young's modulus of the resin. The complex Young's modulus of the resin was estimated from the measurement results using response surfaces of the relationship between the energy velocity, attenuation and the resin complex modulus. It was verified that the estimated storage modulus and loss modulus showed reasonable values and behavior. The development of the anisotropic viscoelastic property of CFRPs can be fully determined in real time using this technique.

1. Introduction

Carbon fiber reinforced plastics (CFRPs) have been used for structural materials in aircrafts and automobiles due to their high specific strength and stiffness. Thermoset CFRPs are generally manufactured by stacking prepreg sheets, which contain carbon fibers and uncured resin. Heat and pressure are applied to the stacked prepregs to cure the resin and exclude air voids. The residual stress induced during molding causes curvature of the manufactured parts. Excess stresses may occur in CFRP parts with a dimensional misalignment after assembly; hence, reduction of the curvature is strongly demanded [1-3]. It has been reported that the curvature of manufactured CFRP parts can be controlled by the profile and distribution of temperature in the cure process [3,4]. It is required to perform a process simulation to search for manufacture conditions that can minimize the curvature.

To perform a process simulation, the development of the anisotropic modulus of a curing CFRP prepreg must be obtained [1,5,6]. Conventionally, the dependence of resin modulus on degree of cure (DOC) has been measured by dynamic mechanical analysis (DMA) tests [7,8]. Preparation of many samples with different DOCs is required for DMA tests. DMA tests are performed for each sample, and a relationship between the elastic modulus of the resin and the DOC is obtained. Although DMA can accurately measure the dynamic modulus of a cured resin, problems arise when the dynamic modulus of an uncured resin is measured. Uncured resins are often so soft that samples cannot maintain their shapes during DMA tests [8]. The cure reaction of an uncured resin proceeds due to the temperature rise in DMA, which also prevents an accurate measurement of the dynamic modulus. Some resins used for CFRP prepregs reach a full cure level in a short time during the standard cure cycle determined by the manufacturer. This may cause an error between the DOC estimated from the temperature profile and that of the prepared sample. Therefore, a method is required to monitor the development of resin modulus during a cure cycle.

Ultrasonic testing has been studied for measurement of the cure-dependent dynamic modulus of resins. Cure monitoring methods that use a pulse-echo or through-transmission technique have been reported [9-13]. The velocity and attenuation of an ultrasonic wave propagating in the through-thickness direction are measured in these techniques. The storage modulus and loss modulus of the resin are calculated by a simple analysis of a one-dimensional wave equation. Some studies have reported the use of an ultrasonic guided wave for cure monitoring. A guided wave propagating in a thin wire waveguide inserted to resin [14] and that propagating in a thin plate have been used for cure monitoring [15,16]. Guided wave techniques have also been applied to cure monitoring of CFRPs [15-17]. However, it is more difficult to link the velocity and attenuation to the viscoelastic property of the tested material in the guided wave methods than in the pulse-echo and through-transmission techniques. The guided wave cure monitoring

* Corresponding author.
E-mail address: mizukami.koichi.tp@ehime-u.ac.jp (K. Mizukami).

https://doi.org/10.1016/j.ultras.2019.105952
Received 7 February 2019; Received in revised form 24 June 2019; Accepted 24 June 2019
Available online 25 June 2019
0041-624X/

technique for CFRPs is often limited to the acquisition of the correlations between the cure level and the velocity and attenuation [15,16]. It is expected that the use of a plate wave will have the advantages of simplicity in sensor placement, cure monitoring of thin plates, and different accessibility compared with the bulk wave methods. The previous study of the authors reported a method to estimate the viscoelastic properties of a CFRP from the energy velocity and attenuation of the guided wave [17]. However, the development of the viscoelastic properties could be obtained after the cure cycle was finished in the previous method. Real-time acquisition of the cure-dependent modulus has not yet been accomplished. Moreover, the energy velocity measured by the experimental setup in the previous study was not so sensitive to the change of the resin modulus. In this study, a new guided wave method is developed for real-time monitoring of the anisotropic viscoelastic properties of CFRPs during the cure cycle. The measurement setup is also improved to enhance the sensitivity of the energy velocity to the resin modulus. First, the energy velocity and attenuation of the guided wave propagating in the transverse direction of a curing CFRP are measured using one transmitter and two receivers. Second, the anisotropic material properties of the CFRP are expressed as functions of the complex modulus of the resin using a micromechanics model of fiber reinforced composites. By combining the micromechanics model and a transfer matrix method, the relationship between the energy velocity, attenuation and complex modulus of the resin is numerically obtained. Third, the development of the complex modulus of the resin is estimated from the measured energy velocity and attenuation using the numerical analysis results.

2. Experiment

2.1. Material and method

Ultrasonic guided waves propagating in a curing CFRP were measured and the energy velocity and attenuation were obtained. Fig. 1 shows the experimental setup for the guided wave measurement. The material under the test was a 12-layer unidirectional CFRP prepreg (Toray Industry, Inc., T700SC/2592) with a size of 250 mm × 250 mm. A breather was mounted on a stainless plate, and then the CFRP prepreg sandwiched by release films on both sides was placed on the breather. It was known in advance that the rate of change of the guided wave velocity became quite small if the breather was not inserted between the bottom release film and stainless plate. Moreover, it was found that the CFRP prepreg was easily warped when cured in vacuum bag without tool plate, which adversely affected the accuracy of the measurement. The experimental setup shown in Fig. 1 can satisfy both sufficiently large change rate of the guided wave velocity and flatness of the CFRP plate during the cure process. Three piezoelectric transducers were placed on the top release film. One transducer was used as a transmitter (T) to generate the ultrasonic guided wave, and two transducers were receivers (R1, R2) to measure the guided wave. The transducers were heat-resistant PZT sensors (Fuji Ceramics Corporation, C-64) with a diameter of 20 mm, thickness of 0.4 mm and Curie temperature of 345 ℃. The row of the sensors was perpendicular to the fiber direction for measurement of the guided wave propagating in the transverse direction of the CFRP. The distance between the sensor T and sensor R1 was 50 mm. The distance between the sensor T and sensor R2 was 80 mm. The layered media and transducers were covered by a vacuum bag to apply pressure to the CFRP prepreg. This pressure enabled the sensors to have good contact with the tested material.

The CFRP prepreg was cured in an electric furnace. Fig. 2 shows the temperature profile for curing. The temperature was increased to 90 ℃ from room temperature at a heating rate of 2 ℃/min. The temperature was then held at 90 ℃ for 5 h. After the isothermal process, the CFRP was cooled to room temperature. The development of the DOC in this temperature profile is shown in Fig. 2. The DOC development was obtained using a differential scanning calorimetry (DSC). The residual heat of the reaction of the uncured prepreg samples was measured to calculate the DOC. The DOC of the CFRP prepreg reached approximately 0.9 at the end of the cure cycle. The gel point of T700SC/2592 prepreg was approximately 0.6. The gelation of the CFRP prepreg occurred at an oven time of approximately 150 min as seen in Fig. 2.

The waveform of the voltage applied to the sensor T from a function

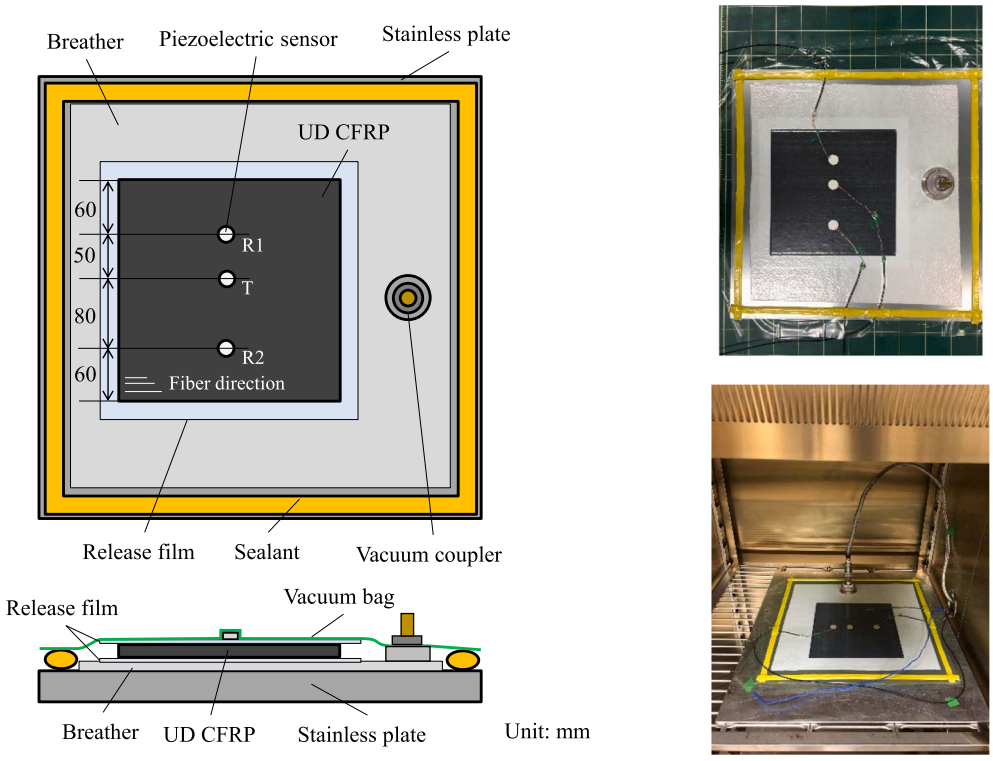

Fig. 1. Experimental setup for ultrasonic guided wave cure monitoring in vacuum bag molding.

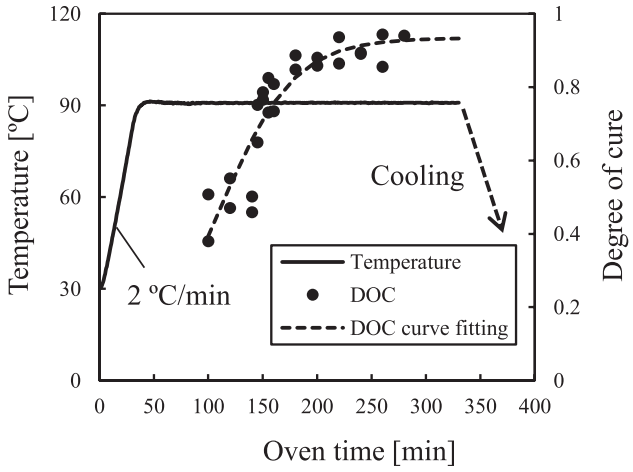

Fig. 2. Temperature profile for curing and development of degree of cure measured by differential scanning calorimetry.

generator (Tektronix, AFG 3000 series) was a Hanning windowed five-cycle burst sine wave with an amplitude of 10Vpp and frequency of 50 kHz. The voltages of receivers R1 and R2 were measured by an oscilloscope (PicoTechnology, Picoscope 5000 series) after passing through a high-pass filter and voltage amplifier (NF Corporation, 5307). The measurement of the guided wave was performed at 30-sec intervals during the cure cycle.

2.2. Results and discussion

The energy velocity and attenuation of the guided wave were obtained by signal processing of the received waveforms. Fig. 3 shows the waveforms of the transmitter and receivers and their signal processing results. Fig. 3(a) shows the voltage waveform applied to the sensor T and its envelope. The envelope was obtained using the Hilbert transform (HT) of the waveform [18,19]. Fig. 3(b) shows an example waveform of the sensors R1 and R2 and their envelopes obtained 200 min after the beginning of heating. The waveforms of the receivers were almost the same as the waveform of the transmitter, which indicated that there was almost no change in the shape of the wave packet resulting from dispersion. Hence, the energy velocity was calculated assuming that the time at which the peak of the envelope was observed was the arrival time of the guided wave. The times at which the envelope of the waveforms of the sensors T, R1 and R2 had the maximum value were defined as t_T, t_{R1} and t_{R2}, respectively. The energy velocity V_e was calculated from Eq. (1).

$$V_e = \frac{L_1}{t_{R1} - t_T} \tag{1}$$

L_1 in Eq. (1) is the distance between the sensors T and R1 (= 50 mm). V_e can be calculated by dividing the distance between the sensors T and R2 by $t_{R2} - t_T$ or dividing the distance between the sensors R1 and R2 by $t_{R2} - t_{R1}$. Although almost the same V_e development curve was obtained by these calculation methods, the scatter of the data certain period of time after the gelation was smallest when V_e was calculated from Eq. (1). Since the resin was highly attenuative around the gel point, the voltage of the R2 was much smaller than that of R1 and masked by electromagnetic noise. The HT for the R2 waveform failed to accurately read its arrival time in this period, while the voltage of R1 was sufficiently larger than the noise level. Fig. 3(c) shows the 50 kHz wavelet coefficients obtained by applying the continuous wavelet transform (CWT) to the receiver waveforms in Fig. 3(b). The attenuation α at 50 kHz was calculated using the maximum values of the wavelet coefficients A_1 and A_2.

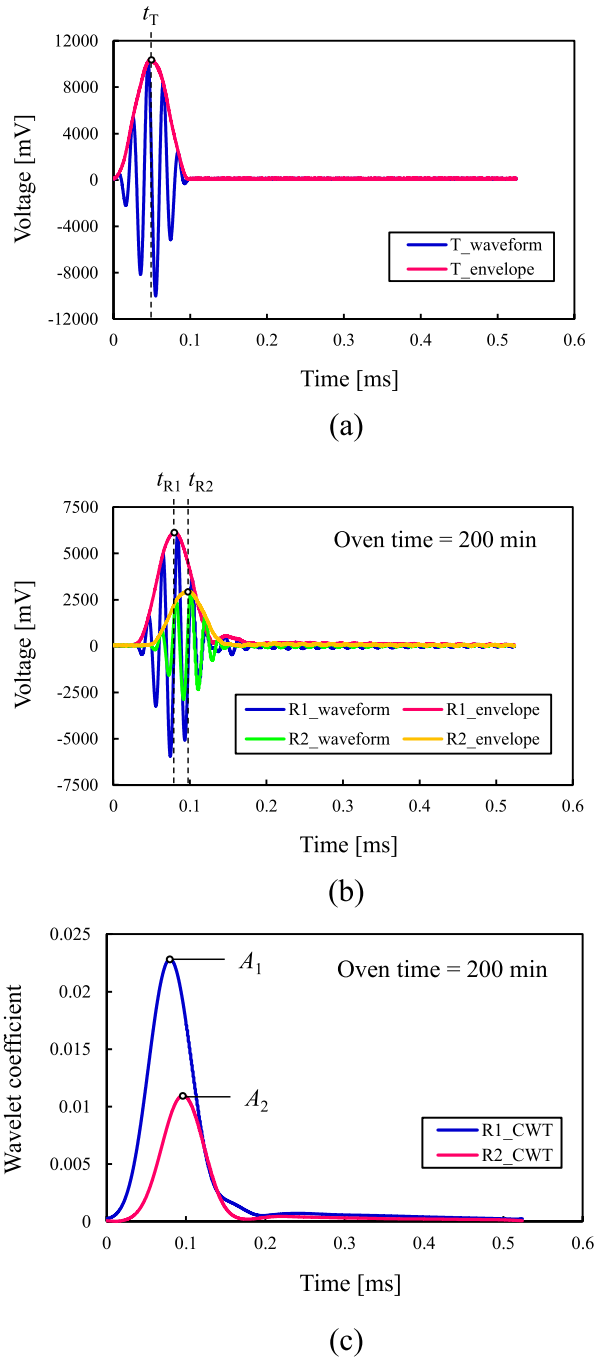

Fig. 3. Measured waveforms and signal processing results. (a) Excitation waveform and its envelope. (b) Received waveforms at oven time of 200 min and their envelopes. (c) 50 kHz wavelet coefficients of received waveforms at 200 min.

$$\alpha = \frac{1}{L_{12}} \ln\left(\frac{A_1\sqrt{L_1}}{A_2\sqrt{L_2}}\right) \tag{2}$$

L_2 is the distance between the sensors T and R2, and $L_{12} = L_2 - L_1$. The attenuation in Eq. (2) is material damping that excludes the effect of geometrical spreading [18,20].

Fig. 4 shows the development of the energy velocity and attenuation of the guided wave obtained in the experiment. The voltage of the receivers was so low until an oven time of 170 min that it was difficult to accurately determine the energy velocity and attenuation. Similar results were also obtained in our previous work when the guided wave propagating in the transverse direction was measured [17]. The energy

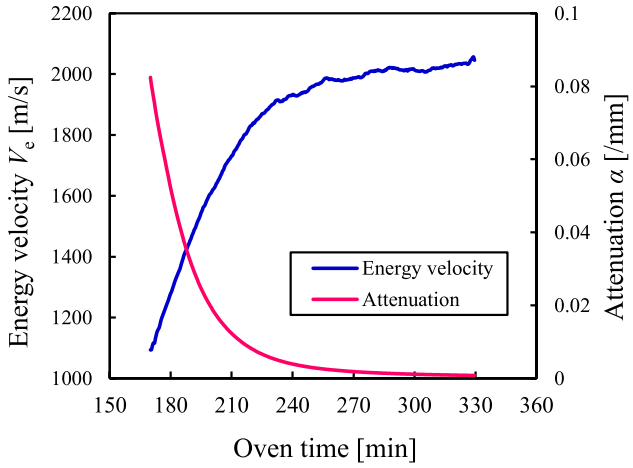

Fig. 4. Energy velocity and attenuation of guided wave obtained from the experiment.

velocity rapidly developed from 170 min to 220 min and then its change rate decreased. The curve of the V_e development was similar to that of the DOC development shown in Fig. 2. Hence, the completion of the cure reaction could be predicted by the observation of the V_e development. The attenuation rapidly decreased from 170 min to 220 min, and its final value was close to zero. According to Fig. 2, gelation occurred at an oven time of approximately 150 min. Therefore, the cure reaction after gelation could be monitored by this method.

3. Numerical analysis

3.1. Micromechanics model

The relationship between the energy velocity, attenuation and anisotropic viscoelastic property of the CFRP was obtained through numerical analyses. The results of the numerical analysis were used to estimate the viscoelastic property of the CFRP from the measurement results. In this study, the cure-dependent anisotropic viscoelastic property of the CFRP was fully estimated from only the energy velocity and attenuation of the guided wave propagating in the transverse direction of the unidirectional CFRP. The carbon fiber is an anisotropic elastic material and its material property does not change during molding. The resin was assumed to be an isotropic viscoelastic material whose material property changes during molding. The material property of a CFRP can be calculated from the material properties of the carbon fiber and resin by using a micromechanics model for fiber reinforced composite. If the material property of the carbon fiber is known, the material property of the CFRP can be expressed by only the material property of the resin. Hence, the energy velocity and attenuation of the guided wave can be expressed as functions of the material property of the resin. The self-consistent model developed by Hashin and Rosen, and Whitney was used as the micromechanics model [21,22]. The material property of a unidirectional CFRP is expressed as follows using this model [2].

$$E_{11} = E_{11f}V_f + E_m(1 - V_f) + \frac{4(\nu_m - \nu_{12f})^2 k_f k_m G_m(1 - V_f)V_f}{(k_f + G_m)k_m + (k_f - k_m)G_m V_f} \tag{3}$$

$$E_{22} = E_{33} = \frac{1}{(1/4k_T) + (1/4G_{23}) + (\nu_{12}^2/E_{11})} \tag{4}$$

$$G_{12} = G_{13} = G_m\left\{\frac{(G_{12f} + G_m) + (G_{12f} - G_m)V_f}{(G_{12f} + G_m) - (G_{12f} - G_m)V_f}\right\} \tag{5}$$

$$G_{23} = \frac{G_m\{k_m(G_m + G_{23f}) + 2G_{23f}G_m + k_m(G_{23f} - G_m)V_f\}}{k_m(G_{23f} + G_m) + 2G_{23f}G_m - (k_m + 2G_m)(G_{23f} - G_m)V_f} \tag{6}$$

$$\nu_{12} = \nu_{13} = \nu_{12f}V_f + \nu_m(1 - V_f) + \frac{(\nu_m - \nu_{12f})(k_m - k_f)G_m(1 - V_f)V_f}{(k_f + G_m)k_m + (k_f - k_m)G_m V_f} \tag{7}$$

$$\nu_{23} = 1 - \frac{E_{22}}{2k_T} - \frac{2\nu_{12}^2 E_{22}}{E_{11}} \tag{8}$$

where,

$$G_m = \frac{E_m}{2(1 + \nu_m)} \tag{9}$$

$$G_{23f} = \frac{E_{33f}}{2(1 + \nu_{23f})} \tag{10}$$

$$k_T = \frac{(k_f + G_m)k_m + (k_f - k_m)G_m V_f}{(k_f + G_m) - (k_f - k_m)V_f} \tag{11}$$

$$k_m = \frac{E_m}{2(1 - \nu_m - 2\nu_m^2)} \tag{12}$$

$$k_f = \frac{E_{33f}}{2(1 - \nu_{23f} - 2\nu_{23f}^2)} \tag{13}$$

V_f is the volume fraction of carbon fibers in the CFRP. E, G, ν and k denote the Young's modulus, shear modulus, Poisson's ratio and bulk modulus, respectively. The subscripts f and m denote the fiber and resin, respectively. The numbers 1, 2 and 3 correspond to fiber, transverse and thickness directions of the unidirectional CFRP, respectively. If the material property of the carbon fiber is known, the material property of the unidirectional CFRP is expressed as a function of Young's modulus E_m and Poisson's ratio ν_m of the resin. The Poisson's ratio of resin is close to 0.5 in a rubbery state and rapidly approaches a constant value as the resin vitrifies [23]. Because only the curing process after gelation could be monitored in the experiment of the guided wave measurement, it was assumed that ν_m was constant in the estimation of the anisotropic modulus of the CFRP from the measurement results. Therefore, the anisotropic elastic property of the CFRP could be expressed as a function of only E_m. Taking the correspondence principle into consideration, the viscoelastic property of the CFRP could be obtained by replacing the elastic modulus E_m in Eqs. (3)–(13) with a complex modulus $E_m' + iE_m''$, where E_m' and E_m'' are the storage modulus and loss modulus of the resin.

3.2. Transfer matrix method

Transfer matrix method is a semi-analytical method that can find the complex phase velocity of the guided wave propagating in a stratified media [24,25]. The energy velocity and attenuation can be calculated once the complex phase velocity is known. Fig. 5 shows the analytical model for the transfer matrix method. The waveguide in the measurement in Fig. 1 was assumed to be a four-layer plate composed of a bottom release film, unidirectional CFRP, top release film and vacuum bag. Since the acoustic impedance of the breather was low, it was assumed that the bottom surface of the waveguide was a free surface. x_1 was the direction of the propagation of the guided wave and x_3 was the through-thickness direction. The plane strain condition was adopted and the model was assumed to be infinitely long in the x_2

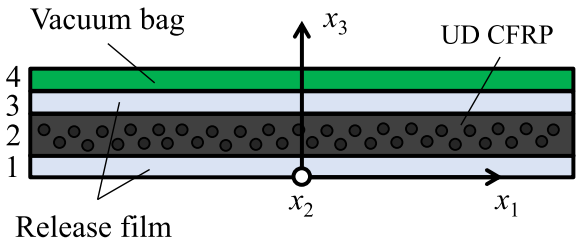

Fig. 5. Analytical model for transfer matrix method.

direction. The guided wave propagating in the material was assumed to be the superposition of the partial waves: quasi-P wave, SH wave and SV wave. Each of the waves is written as follows.

$$u_1 = U_1 \exp(ik^*(x_1 + \gamma x_3 - c_p^* t)) \tag{14}$$

$$u_2 = U_2 \exp(ik^*(x_1 + \gamma x_3 - c_p^* t)) \tag{15}$$

$$u_3 = U_3 \exp(ik^*(x_1 + \gamma x_3 - c_p^* t)) \tag{16}$$

k^* is the complex wave number, and c_p^* is the complex phase velocity. $k^* c_p^*$ is equal to the angular frequency ω. U_1, U_2 and U_3 are constants, and γ is the ratio of the wavenumber in the x_3 direction to that in the x_1 direction. The displacements in three directions are coupled together in general anisotropic materials and waves are superposition of the quasi-P, SH and SV waves. The governing equations were the equation of motion, strain-displacement relationship, and Hooke's law. The material property of the CFRP expressed as a function of the resin complex modulus $E_m' + iE_m''$ was substituted into the stiffness tensor in Hooke's law. By substituting the displacements in Eqs. (14)–(16) into the governing equations, the displacements and stresses at the top and bottom surfaces of the mth layer in the stratified media were linked as the following equation shows.

$$\begin{Bmatrix} \boldsymbol{u} \\ \boldsymbol{\sigma} \end{Bmatrix}_{\mathrm{m,top}} = \begin{bmatrix} \boldsymbol{T}_a^{(\mathrm{m})} & \boldsymbol{T}_b^{(\mathrm{m})} \\ \boldsymbol{T}_c^{(\mathrm{m})} & \boldsymbol{T}_d^{(\mathrm{m})} \end{bmatrix} \begin{Bmatrix} \boldsymbol{u} \\ \boldsymbol{\sigma} \end{Bmatrix}_{\mathrm{m,bottom}} \tag{17}$$

The vector on the left side of Eq. (17) consists of a displacement u and stress σ at the top surface of the mth layer. The vector on the right side is the displacement-stress vector at the bottom surface of the mth layer. The matrix on the right side is the transfer matrix of the mth layer that links the displacements and stresses at the top and bottom surfaces. Taking the continuity of the displacement and stress at the interface, the displacements and stresses at the top and bottom surfaces of the stratified media were linked as follows.

$$\begin{Bmatrix} \boldsymbol{u} \\ \boldsymbol{\sigma} \end{Bmatrix}_{4,\mathrm{top}} = \boldsymbol{T}^{(4)}\boldsymbol{T}^{(3)}\boldsymbol{T}^{(2)}\boldsymbol{T}^{(1)} \begin{Bmatrix} \boldsymbol{u} \\ \boldsymbol{\sigma} \end{Bmatrix}_{1,\mathrm{bottom}} \tag{18}$$

$T^{(m)}$ is the transfer matrix of the mth layer shown in Eq. (17). As Eq. (18) shows, the transfer matrix of the stratified media is the multiplication of the transfer matrices of all layers. Because the stress components in the x_3 direction becomes zero at the free surfaces, Eq. (18) is written as follows.

$$\begin{Bmatrix} \boldsymbol{u} \\ 0 \end{Bmatrix}_{4,\mathrm{top}} = \begin{bmatrix} \boldsymbol{T}_a & \boldsymbol{T}_b \\ \boldsymbol{T}_c & \boldsymbol{T}_d \end{bmatrix} \begin{Bmatrix} \boldsymbol{u} \\ 0 \end{Bmatrix}_{1,\mathrm{bottom}} \tag{19}$$

The matrix on the right side of Eq. (19) is the multiplication of the transfer matrices of all the layers shown in Eq. (18). Because the displacement u has nontrivial solution, the following dispersion equation can be obtained.

$$\det(\boldsymbol{T}_c) = 0 \tag{20}$$

Eq. (20) is an equation with respect to the complex phase velocity c_p^*. c_p^* for a specific frequency can be found by solving this equation. c_p^* is expressed as follows using the real phase velocity c_p and attenuation α [24].

$$\frac{1}{c_p^*} = \frac{1}{c_p} - i\frac{\alpha}{\omega} \tag{21}$$

The attenuation at the frequency ω can be obtained from the imaginary part of the right side in Eq. (21). The energy velocity of the guided wave V_e can be calculated from Eq. (22) after c_p^* is known [26].

$$V_e = \frac{\int_0^h \int_0^{2\pi/\omega} P dt dx_3}{\int_0^h \int_0^{2\pi/\omega} Q dt dx_3} \tag{22}$$

h is the thickness of the stratified plate, P is the Poynting vector, and Q is the sum of the kinetic energy and strain energy.

Table 1
Material properties used for calculation of energy velocity and attenuation.

	Fiber (Carbon fiber)	Resin (EP)	Release film (PTFE)	Vacuum bag (PA)
Elastic modulus [GPa]				
E_{11}	230		0.5	2.0
E_{22} (=E_{33})	18.2			
G_{12} (=G_{13})	36.6			
Poisson's ratio				
ν_{12} (=ν_{13})	0.27	0.35	0.36	0.3
ν_{23}	0.3			
Density [kg/m^3]				
ρ	1600 (CFRP)		2200	1140

3.3. Relationship between energy velocity, attenuation and material property

The relationship between the energy velocity, attenuation and Young's modulus of the resin under the experimental condition was determined by using the micromechanics model and transfer matrix method. Table 1 shows the material properties used for the calculation. In the material property of the carbon fiber, 1 is the longitudinal direction of the fiber, and 2 and 3 are the directions perpendicular to the fiber. The fiber volume fraction V_f was assumed to be 60 %. Generally, V_f slightly increases during molding. However, since the thickness change caused by the vacuum pressure and cure shrinkage was not significant compared with the change of the material property, V_f and density of the CFRP was assumed to be constant during the cure cycle. Since the thickness of the prepreg was 0.14 mm, the thickness of the 12-layer CFRP was assumed to be 1.68 mm in the calculations. The average thickness of the sample measured after curing was 1.63 mm, which indicated that the change of the thickness was negligibly small. The thickness of the release film and vacuum bag was 0.05 mm. The elastic modulus in the transverse direction of the cured CFRP was measured by a tensile test at room temperature, and the measured value was 8.2 GPa. According to the micromechanics model, the Young's modulus of the resin for this transverse modulus was estimated to be 3.23 GPa. Thus, calculations of the energy velocity and attenuation were performed for E_m' less than 3.5 GPa.

The energy velocity and attenuation at 50 kHz were calculated. Only the lowest order modes, that is, two P + SV modes and one SH mode were observed at this frequency. Fig. 6 shows examples of the dispersion curves of the energy velocity of the guided wave. Fig. 6(a)–(c) are dispersion curves for E_m = 0.5, 1.5 and 2.5 GPa, respectively. In the calculations to obtain the results in Fig. 6, the loss modulus of the resin was assumed to be zero. As Fig. 6 shows, the fastest mode around 50 kHz was the P + SV1 mode for any E_m. More importantly, there was almost no dispersion of the P + SV1 mode around 50 kHz. These characteristics of the P + SV1 mode were maintained even when a realistic value of the loss modulus was taken into consideration for the calculation. Because the P + SV1 mode was dominant in the experiment to obtain Fig. 4, the energy velocity and attenuation of this mode were numerically obtained for various complex moduli. Fig. 7 shows the calculation results of the energy velocity and attenuation of the P + SV1 mode at 50 kHz. The energy velocity increased with E_m', and the contribution of E_m'' became smaller at a larger E_m'. The attenuation increased with E_m'' and approached zero as E_m' increased.

The response surfaces of the energy velocity and attenuation were produced to express the relationships in Fig. 7 as formulae [17,27]. The response surface of the energy velocity was a third-order polynomial with two variables as shown in Eq. (23).

$$y = \beta_0 + \beta_1 x_1 + \beta_2 x_2 + \beta_3 x_1^2 + \beta_4 x_1 x_2 + \beta_5 x_2^2 + \beta_6 x_1^3 + \beta_7 x_1^2 x_2 + \beta_8 x_1 x_2^2 + \beta_9 x_2^3 \tag{23}$$

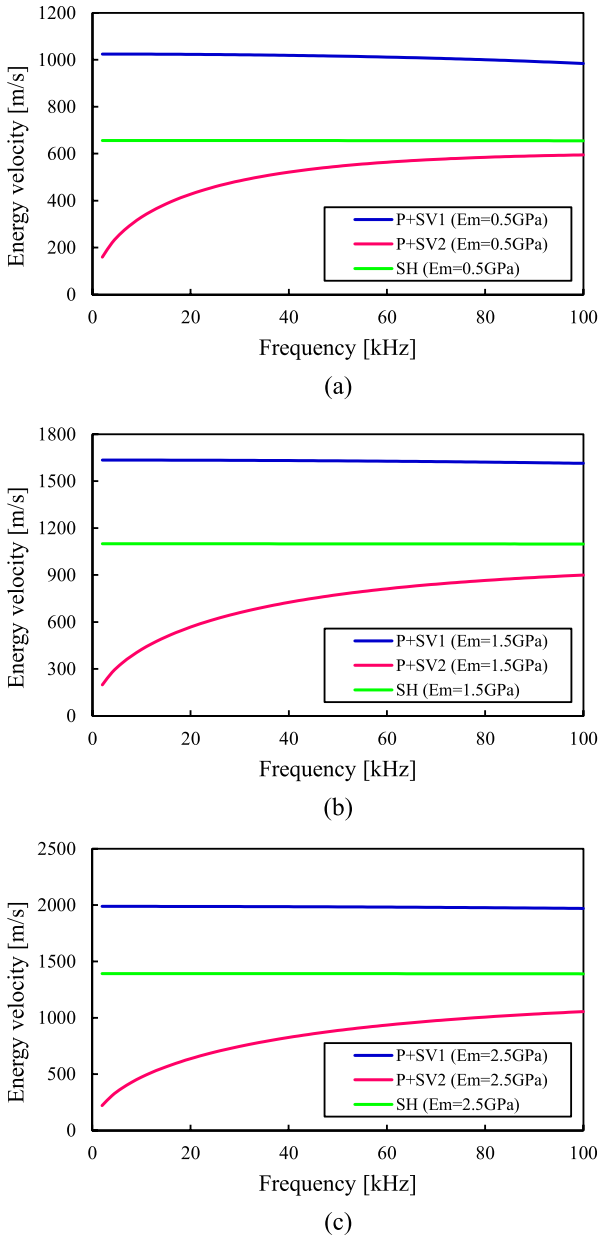

Fig. 6. Examples of dispersion curves of energy velocity for the stratified media. (a) E_m = 0.5 GPa. (b) E_m = 1.5 GPa. (c) E_m = 2.5 GPa.

In Eq. (23), y is an output, and x_1 and x_2 are input variables. y, x_1 and x_2 are the energy velocity, storage modulus and loss modulus, respectively. β_i are coefficients of the polynomial. The response surface of the attenuation was produced using the following equation.

$$y = x_2^{\beta_{10}} \exp(\beta_0 + \beta_1 x_1 + \beta_2 x_2 + \beta_3 x_1^2 + \beta_4 x_1 x_2 + \beta_5 x_2^2 + \beta_6 x_1^3 + \beta_7 x_1^2 x_2 + \beta_8 x_1 x_2^2 + \beta_9 x_2^3) \quad (24)$$

In Eq. (24), y, x_1 and x_2 are the attenuation, storage modulus and loss modulus, respectively. The coefficients β_i were determined such that the squared error between the numerical results in Fig. 7 and the response surface was minimized. The adjusted R-square value was larger than 0.999 for both response surfaces, which indicates the validity of the approximate functions in Eqs. (23) and (24). Therefore, the formulae of the relationship between the energy velocity, attenuation and complex modulus of the resin were obtained.

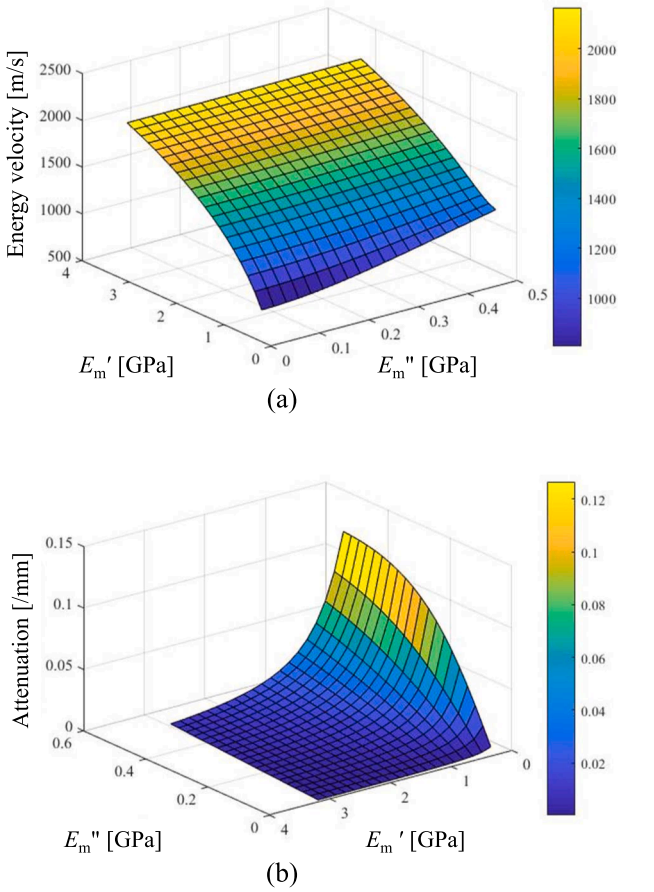

Fig. 7. Numerically obtained relationship between energy velocity and attenuation of 50 kHz P + SV1 mode and resin complex modulus. (a) Energy velocity. (b) Attenuation.

4. Inverse analysis

The development of the complex modulus of the resin was estimated from the measurement results using the response surfaces. The complex modulus was estimated by finding the combination of the storage modulus and loss modulus that minimized the squared error between the response surface and measurement results. An optimization algorithm, based on the least squares method, was used to find the solution. The storage modulus and loss modulus were estimated at each time in the curing process. Since the computational cost for solving Eq. (20) is large, the response surface was necessary for real-time estimation of the complex modulus. Fig. 8 shows the estimated development of the Young's modulus of the resin during the cure cycle. The storage modulus increased as the resin was cured and reached the final value of approximately 2.7 GPa. This was the storage modulus at 90 °C. Measurement of the energy velocity was performed for the cured CFRP sample at room temperature to verify the inverse analysis. The storage modulus of the cured resin was estimated from the measured energy velocity assuming that the loss modulus was zero. Table 2 shows the comparison of the Young's modulus at room temperature estimated by the tensile test and guided wave method. The storage modulus of the resin at room temperature was estimated to be 2.95 GPa. Because the tensile test showed that the Young's modulus of the cured resin was 3.23 GPa at room temperature, the estimated Young's moduli were in good agreement. Fig. 8 shows that the loss modulus decreased during the cure process after the peak at 190 min. This was a typical behavior of a curing resin. However, it should be noted that the estimated loss modulus is sensitive to the error of the attenuation in the final stage of cure. The dependence of the complex modulus on the DOC was

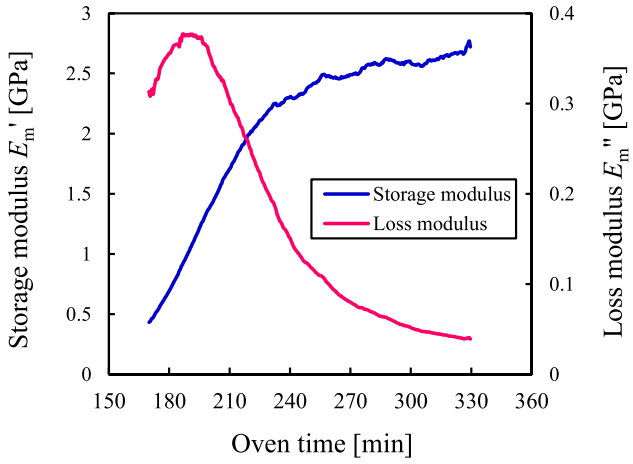

Fig. 8. Development of complex modulus of resin estimated by measurement results and response surfaces.

Table 2
Comparison of the elastic modulus of the resin estimated from the results of the tensile test and guided wave measurement for the cured CFRP at room temperature.

Method	Estimated Young's modulus [GPa]
Tensile test	3.23
Guided wave measurement	2.95

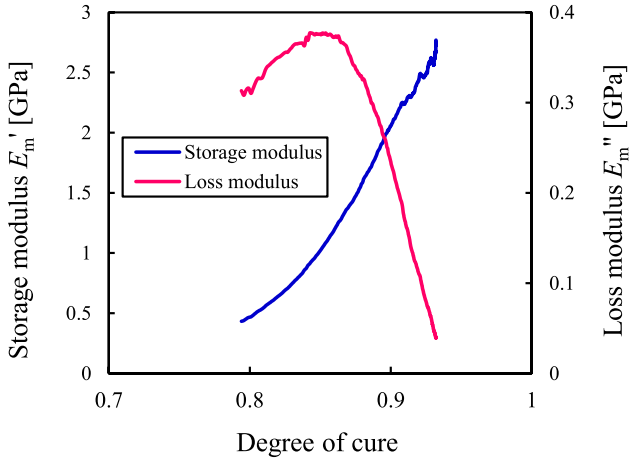

Fig. 9. Relationship between complex modulus of resin and degree of cure.

obtained using the development of the DOC in Fig. 2 and the estimation results in Fig. 8. Fig. 9 shows the relationship between the complex modulus of the resin and DOC. It was possible for the guided wave cure monitoring to estimate the resin complex modulus for a DOC larger than 0.79. In process simulations to predict residual stresses, generally, the modulus-DOC relationship after gelation (DOC = 0.6 for T700SC/2592 prepreg) is used. The low modulus at low DOC has a small contribution to the residual stress development. Although the relationship in Fig. 9 was obtained for the limited range of the DOC, it can be a useful material property for process simulation. By substituting the estimated complex modulus of the resin into the equations of the micromechanics, the anisotropic viscoelastic property of the CFRP can be fully determined. It should be noted that the results in Fig. 9 corresponded to the modulus at 50 kHz. Modeling of the viscoelasticity considering the effect of the frequency is required to use the cure monitoring data for an accurate prediction of residual stresses.

5. Conclusion

An ultrasonic guided wave monitoring method was developed to estimate the development of the viscoelastic property of a curing CFRP. The guided wave propagating in the transverse direction of the CFRP prepreg could be measured after gelation. The energy velocity and attenuation of the guided wave were obtained by applying the Hilbert transform and continuous wavelet transform to the waveforms of two receivers.

The anisotropic material property of the CFRP was expressed as a function of only the Young's modulus of the resin using the micromechanics of the fiber reinforced composite. A transfer matrix method was used to calculate the energy velocity and attenuation for a given material property of a CFRP. The relationship between the energy velocity, attenuation and complex modulus of resin was obtained by using a micromechanics model. The energy velocity and attenuation were expressed as a function of the storage modulus and loss modulus of the resin using a response surface methodology.

The development of the resin complex modulus was estimated from the measured energy velocity and attenuation using the produced response surface. The estimated development of the complex modulus showed a reasonable behavior of curing resin. The validity of the method was verified by the comparison of the Young's modulus estimated from the results of the mechanical testing and guided wave technique. Finally, the DOC-dependent complex modulus of the resin was obtained using the results of the modulus estimation and the DOC development measured by a DSC. The cure-dependent anisotropic viscoelastic property of the CFRP could be fully determined by substituting the estimated complex modulus into the micromechanics model.

The cure monitoring method developed in this study can estimate the development of the modulus of CFRPs after gelation. Because the modulus after gelation has a dominant contribution to the residual stress development, the material property estimated by this monitoring technique can be useful as an input for a process simulation of CFRPs. For a precise prediction of the residual stress, a viscoelastic model that takes the effect of the guided wave frequency into consideration is required.

Acknowledgment

This research was supported by Cross-ministerial Strategic Innovation Promotion Program (SIP) of Japan Science and Technology Agency (JST).

References

[1] Travis A. Bogetti, John W. Gillespie, Process-induced stress and deformation in thick-section thermoset composite laminates, J. Compos. Mater. 26 (5) (1992) 626–660.
[2] Shu Minakuchi, Shoma Niwa, Kazunori Takagaki, Nobuo Takeda, "Composite cure simulation scheme fully integrating internal strain measurement", Compos. A 84 (2016) 53–63.
[3] S.R. White, H.T. Hahn, Process modeling of composite materials: residual stress development during cure. Part I. model formulation, J. Compos. Mater. 26 (16) (1992) 2402–2422.
[4] Daniel J. O'Brien, Patrick T. Mather, Scott R. White, Viscoelastic properties of an epoxy resin during cure, J. Compos. Mater. 35 (10) (2001) 883–904.
[5] Oleksandr G. Kravchenko, Chunyu Li, Alejandro Strachan, Sergii G. Kravchenko, R. Byron Pipes, Prediction of the chemical and thermal shrinkage in a thermoset polymer, Compos. A 66 (2014) 35–43.
[6] Oleksandr G. Kravchenko, Sergii G. Kravchenko, R. Byron Pipes, Chemical and thermal shrinkage in thermosetting prepreg, Compos. A 80 (2016) 72–81.
[7] Yeong K. Kim, Scott R. White, Stress relaxation behavior of 3501–6 epoxy resin during cure, Polym. Eng. Sci. 36 (23) (1996) 2852–2862.
[8] Keiji Ogi, Mitsuyoshi Tsutsumi, Koichi Mizukami, Hiroaki Matsutani, Narumichi Sato, Effect of degree of cure on relaxation modulus of thermosetting resin, J. Japan Soc. Compos. Mater. 44 (5) (2018) 183–194.
[9] A. Maffezzoli, E. Quarta, V.A.M. Luprano, G. Montagna, L. Nicolais, Cure monitoring of epoxy matrices for composites by ultrasonic wave propagation, J. Appl. Polym. Sci. 73 (10) (1999) 1969–1977.
[10] M. Rath, J. Döring, W. Stark, G. Hinrichsen, Process monitoring of moulding

compounds by ultrasonic measurements in a compression mould, NDT E Int. 33 (2000) 123–130.
[11] Francesca Lionetto, Alfonso Maffezzoli, Monitoring the cure state of thermosetting resins by ultrasound, Materials 6 (9) (2013) 3783–3804.
[12] V. Koissin, A. Demčenko, V.A. Korneev, Isothermal epoxy-cure monitoring using nonlinear ultrasonics, Int. J. Adhes. Adhes. 52 (2014) 11–18.
[13] Nacef Ghodhbani, Pierre Maréchal, Hugues Duflo, Ultrasound monitoring of the cure kinetics of an epoxy resin: identification, frequency and temperature dependence, Polym. Test. 56 (2016) 156–166.
[14] T. Vogt, M. Lowe, P. Cawley, Cure monitoring using ultrasonic guided waves in wires, J. Acoust. Soc. America 114 (3) (2003) 1303–1313.
[15] S. Pavlopoulou, C. Soutis, W.J. Staszewski, Cure monitoring through time–-frequency analysis of guided ultrasonic waves, Plast., Rubber Compos. 41 (2012) 180–186.
[16] Tyler B. Hudson, Fuh-Gwo Yuan, Automated in-process cure monitoring of composite laminates using a guided wave-based system with high-temperature piezoelectric transducers, ASME J. Nondestruct. Evaluat. 1 (2) (2018).
[17] Koichi Mizukami, Shingo Yoshimoto, Keiji Ogi, In-process acquisition of cure-dependent viscoelastic properties of carbon fiber reinforced composites using micromechanics-based guided wave analysis, Polym. Test. 65 (2018) 459–467.
[18] Konstantin J. Schubert, Axel S. Herrmann, On attenuation and measurement of Lamb waves in viscoelastic composites, Compos. Struct. 94 (2011) 177–185.
[19] Matthieu Gresil, Victor Giurgiutiu, Prediction of attenuated guided waves propagating in carbon fiber composites using Rayleigh damping model, J. Intell. Mater. Syst. Struct. 26 (16) (2015) 2151–2169.
[20] Kassahun Asamene, Larry Hudson, Mannur Sundaresan, Influence of attenuation on acoustic emission signals in carbon fiber reinforced polymer panels, Ultrasonics 59 (2015) 86–93.
[21] Zvi Hashin, B. Walter Rosen, The elastic moduli of fiber-reinforced materials, J. Appl. Mech. 31 (2) (1964) 223–232.
[22] J.M. Whitney, Elastic moduli of unidirectional composites with anisotropic filaments, J. Compos. Mater. 1 (2) (1967) 188–193.
[23] Nuri Ersoy, Tomasz Garstka, Kevin Potter, Michael R. Wisnom, David Porter, Martin Clegg, Graeme Stringer, Development of the properties of a carbon fibre reinforced thermosetting composite through cure, Composites: Part A Appl. Sci. Manufact. 41 (2010) 401–409.
[24] Joseph L. Rose, Ultrasonic Guided Waves in Solid Media, Cambridge University Press, 2014.
[25] Michel Castaings, Bernard Hosten, Guided waves propagating in sandwich structures made of anisotropic, viscoelastic, composite materials, J. Acoust. Soc. America 113 (5) (2003) 2622–2634.
[26] A. Bernard, M.J. Lowe, Guided waves energy velocity in absorbing and non-absorbing media, J. Acoust. Soc. America 110 (1) (2001) 186–196.
[27] Akira Todoroki, Tetsuya Ishikawa, Design of experiments for stacking sequence optimizations with genetic algorithm using response surface approximation, Compos. Struct. 64 (2004) 349–357.